БЪЛГАРСКА АКАДЕМИЯ НА НАУКИТЕ • BULGARIAN ACADEMY OF SCIENCES
GEOCHEMISTRY, MINERALOGY AND PETROLOGY • 43 • SOFIA • 2005

Au-Ag-Te-Se deposits
IGCP Project 486, 2005 Field Workshop, Kiten, Bulgaria, 14-19 September 2005

Mineral assemblages from the vein salband at Sacarimb, Golden Quadrilateral, Romania: I. Sulphides and sulphosalts

Cristiana L. Ciobanu[1], Nigel J. Cook[2], Nicu Capraru[3], Gheorghe Damian[4], Petru Cristea[3]

[1]Department of Earth Sciences, University of Adelaide, North Terrace, Adelaide, South Australia; [2]Natural History Museum Geology, University of Oslo, Norway; [3]Deva Gold S.A., Certeju de Sus, Romania; [4]Universitatea de Nord, Baia Mare, Romania

Abstract: Sb- and As-sulphosalts are abundant within salband ores from the Sacarimb epithermal Au-Te vein system, South Apuseni Mts., Romania. Similar to the main ore, tetrahedrite-tennantite, bournonite-seligmannite and jordanite-geocronite are the three main groups, although the first group is prominent in the salband, whereas the second prevails in the vein filling. Various Ag- and/or Cu- bearing Bi sulphosalts are also identified and documented here for the first time. These include cosalite, aikinite, lillianite homologues and members of the galena-matildite series. Sulphosalts are the main carriers for a first population of tellurides. Reopening of the veins is interpreted from a range of brecciation textures typified by 'emulsion-like' halos surrounding the sulphide/sulphosalt grains. Deposition a second population of tellurides is associated with this event; Bi-sulphosalts relates to this episode only.

Key words: Sacarimb, Romania, epithermal Au-Te mineralization, Bi-sulphosalts

Introduction

Sacarimb is an epithermal Au-Te vein system of Neogene age in the Golden Quadrilateral, South Apuseni Mts., Romania. Ca. 32 t of gold was mined from the Sacarimb deposit between the early 18th Century and 1992; more than half of the gold was present as tellurides, notably nagyagite, sylvanite and petzite. High-grade ores are worked out, and the remaining resource outlined by Deva Gold S.A. in recent years consists mostly of smaller, low-grade veins and vein margin (salband) mineralization. As part of continuing work targeting the telluride mineralogy at Sacarimb (Ciobanu et al., 2004), we aim here to give a first account of mineralogy in the salband ore. We will emphasise the notable similarities and differences between the salband mineralization and the major veins, and also provide the first confirmation on the presence of Bi-sulphosalts in the Sacarimb ore.

Sample description

The present suite of samples (Table 1) is representative of the vein margins across a 300 m vertical interval, i.e., from Carol (477 m) to Maria levels (773 m) (Fig. 1 in Cook et al., this volume).

Our data indicate that, in the majority of the samples, the main mineral assemblage consists of sulphides (pyrite, sphalerite and

galena), and sulphosalts, i.e., members of the tetrahedrite-tennantite (Td-Tn; Table 2), bournonite-seligmannite (Bnn-Sel; Table 3) and jordanite-geocronite (Jord-Gcn; Table 3) series. Pyrite is generally the dominant sulphide and tetrahedrite-tennantite the main sulphosalt. Alabandite can form cm-sized nodules and/or bands and may also be part of the other samples in variable proportions, mainly observed where sphalerite is prominent over pyrite. Rhodochrosite and/or quartz are the main gangue minerals. Sericite is present in variable amounts, mostly after feldspars in the host rock andesite. Minor components are apatite, rutile, barite, and gypsum/anhydrite.

Importantly, tellurides are ubiquitous as 10-20 µm inclusions (exceptionally up to 100 µm) within sulphides/sulphosalts from all samples, with the exception of those in which alabandite is dominant. The sample richest in tellurides is one in which the main association consists of pyrite and fahlore (S7.9). It is also here that Bi-sulphosalts are identified. They are also found in abundance in a second sample with a similar pyrite-fahlore assemblage (S7.5).

Textural relationships

Typically, a mottled texture is seen between the sulphides/sulphosalts themselves and/or quartz (Fig. 1A-C). Chemical variation in sulphides/ sulphosalts is observed relating to textural characteristics and the presence of a buffering mineral in the assemblage. For example, sphalerite forming the mottled texture with alabandite (Fig. 1C) has 20.7 wt.% MnS. In the same sample, sphalerite with only 6.3 MnS wt.% forms emulsion bodies within quartz (Fig. 1D). The latter value is closer to the average of MnS content (up to 12 wt.% MnS) in sphalerite from samples that lack alabandite (Fig. 1E).

With the exception of alabandite, each of the other main sulphides/sulphosalts hosts exsolutions of sulphosalts or vica versa. (e.g., sphalerite in fahlore; Table 1).

Table 1. Mineral assemblages in studied samples from Sacarimb

Sample	Location	Sulphides	Sulphosalts	Tellurides	Tell. host	Exsolutions	Gangue
Saca 7.10 (1-Abn)	Maria/773m Dump	Abn, Sp, Py	Td, Stb	NO			Rdc, Qz, Mn-oxide
Saca 7.4	Weisse vein (Bernat/710m)	Abn, Sp, Gn, Py	Jord, Td, Stb	NO			Qz, Rdc
Saca 7.6	Weisse vein (Bernat/710m)	Sp, Gn, Py	Bnn, Jord, Gtd	Nag	Bnn	Jord/Gn	Qz, Rdc, Ser
Saca 7.11 (2-Cal)	Antierzbau vein Bernat/710m	Py, Gn	Bnn, Td	Hs/Stz, Syl	Bnn		Cal
Saca 7.1	Daniel/687m Dump	Py, Sp, Gn	Td, Bnn, Jord	Nag, Syl?, Te?	Sp, Td	Bnn/Td	Qz, Rdc, Ser, Anh/Gyp, Ru
Saca 7.2	Daniel/687m Dump	Py, Sp, Gn	Td, Bnn, Jord	Nag	Td	Jord/Gn, Td/Py	Qz, Rdc
Saca 7.3	Daniel/687m Dump	Sp, Abn, Py, Gn	Td, Bnn	Nag, Te	Gn, Td		Qz, Rdc
Saca 7.7	Daniel/687m Dump	Sp, Py, Gn, Abn	Td, Bnn, Jord	Nag	Jord	Jord/Gn	Qz, Rdc, Ap
Saca 7.5	Daniel/687m Dump	Py, Sp, Gn, (Cc)	Td, (Gfd), Bnn, Bi-ss, Jord, Gtd	Nag, Ttd, Tbs, Buck, Pb-Bi-Te-S, Co	Td, Py, Bnn, Bi-ss	Td/Py, Jord/Nag	Qz, Rdc
Saca 7.8 (4-Rdc)	Ferdinand/ 627m Dump	Sp, Py, Gn, Abn	Td, Bnn, Jord	Nag, Buck?, Syl?, Sdl	Jord	Gn/Jord	Qz, Rdc, Ser, Ap Bar, Anh/Gyp
Saca 7.9 (3-Qz+tell)	Carol/477m Dump	Py, Sp, Gn, (Cc)	Td, Bnn, Bi-ss	Nag, Hs, Pz, Syl	Py, Td	Sp/Td	Qz

Mineral abbreviations: Abn – alabandite, Anh – anhydrite, Ap – apatite, Bar – barite, Bi-ss – bismuth sulphosalts, Bnn – bournonite, Buck – buckhornite, Cc – chalcocite, Co – coloradoite, Gfd – goldfieldite, Gn – galena, Gtd – guettardite, Gyp – gypsum, Hs – hessite, Jord – jordanite, Nag – nagyagite, Pb-Bi-Te-S – aleksite group mineral (?), Py – pyrite, Pz – petzite, Qz – quartz, Rdc – rhodochrosite, Ru – rutile, Sdl – saddlebackite, Ser – sericite, Sp – sphalerite, Stb – stibnite, Stz – stützite, Syl – sylvanite, Tbs – tellurobismuthite, Td – tetrahedrite, Te – native tellurium, Ttd – tetradymite

Table 2. Composition of 'fahlore' minerals, Sacarimb

		Ag	Cu	Pb	Fe	Zn	Mn	Bi	Sb	As	Te	Se	S	Total
	Tetrahedrite-tennantite													
1	S7.9 (mean of 5)	1.38	40.14	-	1.26	8.05	-	-	15.42	8.21	0.19	0.41	23.79	98.84
2	S7.5.11	1.31	36.72	2.82	-	4.89	2.73	2.84	3.69	13.31	2.95	-	26.55	97.82
3	S7.4.1	8.54	29.14	-	1.10	5.16	2.19	-	23.26	4.43	1.95	0.42	23.70	99.89
4	S7.4.2	7.36	29.97	0.77	1.82	7.70	1.56	-	13.36	9.29	0.37	0.68	26.64	99.52
5	S7.11.6	1.98	35.67	-	1.02	6.56	1.39	0.49	24.91	3.32	0.16	0.77	23.74	100.01
6	S7.a5.3	2.88	28.04	2.85	5.68	3.70	4.12	4.21	19.32	2.64	1.67	-	24.39	99.50
7	S7.3 (mean of 6)	2.52	32.34	1.95	0.32	6.65	1.14	0.04	23.29	5.81	0.87	0.29	24.58	99.80
8	S7.8 (mean of 2)	1.03	38.81	0.57	0.49	8.35	-	0.09	13.82	9.65	-	0.19	25.42	98.40
9	S7.1 (mean of 3)	0.89	38.29	0.26	0.51	6.27	1.09	0.18	23.14	3.60	0.70	0.32	23.30	98.48
10	S7.2 (mean of 2)	2.10	37.89	1.35	1.04	6.97	1.09	-	19.72	5.25	0.31	0.24	23.76	99.69
11	S7.10.4	2.97	33.56	-	0.65	7.68	4.11	-	19.41	6.65	0.24	-	24.31	99.58
	Goldfieldite													
12	S7.5.10	1.47	41.45	-	-	2.30	-	2.16	1.49	6.98	14.17	0.32	25.53	95.88
	Pb-Bi-rich goldfieldite (?)													
13	S7.b5 (mean of 2)	6.07	33.90	7.27	3.01	-	0.97	13.61	1.43	-	15.77	-	18.43	100.46

	Formula	% Tetr	% Tenn	% Bi-tetr	% Goldf
1	$(Cu_{10.31}Ag_{0.20}Zn_{1.98}Fe_{0.45})_{12.95}(Sb_{1.94}As_{1.89}Te_{0.02})_{3.85}(S_{12.10}Se_{0.10})_{12.20}$	31-69	31-68	0	0-1
2	$(Cu_{9.31}Ag_{0.22}Pb_{0.22}Zn_{1.20}Mn_{0.80})_{11.73}(As_{2.86}Sb_{0.49}Bi_{0.22}Te_{0.37})_{3.94}S_{13.33}$	12	73	6	9
3	$(Cu_{7.89}Ag_{1.36}Zn_{1.36}Mn_{0.69}Fe_{0.34})_{11.63}(Sb_{3.29}As_{1.02}Te_{0.26})_{4.57}(S_{12.71}Se_{0.09})_{12.80}$	72	22	0	6
4	$(Cu_{7.61}Ag_{1.10}Pb_{0.06}Zn_{1.90}Mn_{0.46}Fe_{0.53})_{11.65}(As_{2.00}Sb_{1.77}Te_{0.05})_{3.82}(S_{13.40}Se_{0.14})_{13.54}$	46	53	0	1
5	$(Cu_{9.43}Ag_{0.31}Zn_{1.69}Mn_{0.43}Fe_{0.31})_{12.16}(Sb_{3.44}As_{0.74Bi0.04}Te_{0.02})_{4.24}(S_{12.44}Se_{0.16})_{12.60}$	81	17	1	1
6	$(Cu_{9.52}Ag_{0.45}Zn_{0.96}Mn_{1.28}Fe_{1.73})_{12.18}(Sb_{2.70}As_{0.60Bi0.34}Te_{0.22})_{3.87}S_{12.95}$	70	15	9	6
7	$(Cu_{8.60}Ag_{0.40}Pb_{0.16}Zn_{1.72}Mn_{0.35}Fe_{0.10})_{11.32}(Sb_{3.23}As_{1.31}Te_{0.11})_{4.66}(S_{12.95}Se_{0.06})_{13.02}$	49-87	10-47	0	0-7
8	$(Cu_{9.86}Ag_{0.15}Pb_{0.04}Zn_{2.06}Fe_{0.14})_{12.25}(Sb_{1.83}As_{2.08}Bi_{0.01})_{3.92}(S_{12.79}Se_{0.04})_{12.83}$	44-49	51-56	0	0
9	$(Cu_{10.20}Ag_{0.14}Pb_{0.02}Zn_{1.63}Mn_{0.34}Fe_{0.15})_{12.47}(Sb_{3.22}As_{0.81}Bi_{0.01}Te_{0.09})_{4.14}(S_{12.31}Se_{0.07})_{12.38}$	75-92	4-34	0-1	0-3
10	$(Cu_{9.91}Ag_{0.32}Pb_{0.11}Zn_{1.77}Mn_{0.33}Fe_{0.31})_{12.75}(Sb_{2.69}As_{1.16}Te_{0.04})_{3.89}(S_{12.31}Se_{0.05})_{12.36}$	46-93	6-52	0	0-2
11	$(Cu_{8.04}Ag_{0.44}Zn_{1.88}Mn_{1.20}Fe_{0.19})_{11.75}(Sb_{2.55}As_{1.42}Te_{0.03})_{4.01}S_{13.24}$	64	35	0	1
12	$(Cu_{10.95}Ag_{0.23}Zn_{0.59})_{11.77}(Te_{1.86}As_{1.56}Sb_{0.21}Bi_{0.17})_{3.81}(S_{13.36}Se_{0.07})_{13.43}$	5	41	5	49
13	$(Cu_{9.90}Ag_{1.10}Fe_{1.05}Mn_{0.34})_{13.08}(Te_{2.41}Sb_{0.23}Bi_{1.27})_{3.91}S_{12.01}$	6	0	32	62

The galena-jordanite pair is most frequently observed (Fig. 1F). Exsolutions in galena are close to end-member jordanite, whereas galena is typically exsolved from intermediate members of the jordanite series (e.g., $Jord_{42-32}$). The two end-members of the series were also observed together (Fig. 1G), with compositions close to geocronite ($Jord_{7.5}$) present at the margin of galena with exsolutions of $Jord_{100}$.

Replacement of sphalerite by galena (Fig. 1H) follows an initial equilibrium relationship, as seen by the carries texture between the two sulphides. Both sphalerite and galena are observed replacing pyrite (Fig. 1E, I). We note rotational trends of replacement in both situations. Zonation patterns in pyrite (Fig. 1J) are frequent and are marked by As-contents up to several wt.%; they often show overgrowth by smaller pyrite grains.

Fields of sulphide/sulphosalt inclusions are observed mainly in pyrite and tetrahedrite. They extend outside grain boundaries as a surrounding halo with typical 'emulsion-like' texture impregnating gangue minerals (Fig. 1K, L). The inclusion shapes are mostly bleb-like; composition is often sphalerite, tetrahedrite or both (Fig. 1D). Such fields of inclusions differ from exsolutions because they are associated with shear-assisted brecciation features (Fig. 1K, L). Brecciation is also marked by areas of diffuse interaction between pyrite and sphalerite (Fig. 1M-O). The sphalerite present as exsolved bodies along the compositional zones in adjacent tetrahedrite (Fig. 1M) is remobilised within the pyrite (Fig. 1N). The boundaries between sphalerite and pyrite are diffuse and clustered by fluid inclusions (Fig. 1O). Importantly, telluride deposition is also associated with such episodes of brecciation.

Table 3. Representative compositions of Pb-Sb-As sulphosalts, Sacaramb

		Ag	Cu	Pb	Fe	Bi	Sb	As	Te	Se	S	Total
	Bournonite-seligmannite											
1	S7.6.8	-	11.27	41.71	-	0.57	9.00	12.47	2.52	-	20.55	98.09
2	S7.6.10	0.77	11.72	44.16	-	-	15.11	5.43	0.91	-	18.80	96.90
3	S7.6.12	1.66	11.55	38.80	-	-	21.46	3.23	2.43	0.65	18.83	98.61
4	S7.6.16	-	12.44	41.36	-	-	22.31	2.07	0.64	0.29	19.66	98.77
5	S7.11.4	-	12.73	43.60	-	-	18.02	4.97	0.84	0.92	18.92	100.00
6	S7.11.5	0.44	12.14	39.87	-	1.14	21.19	2.50	1.97	1.05	19.12	99.42
7	S7.2.2	-	14.71	43.49	-	-	8.18	11.04	0.26	0.75	18.93	97.36
8	S7.2.5	-	13.36	44.19	-	-	5.97	12.71	-	1.23	18.54	96.00
	Jordanite-geocronite											
9	S7.7.1	0.19	-	70.79	0.14	0.16	-	10.65	-	0.19	17.44	99.56
10	S7.7.4.3	-	-	67.24	-	-	3.96	8.04	0.30	0.40	16.51	96.45
11	S7.6.2	-	-	65.51	-	-	7.29	5.83	1.01	0.46	15.94	96.04
12	S7.7.6.13	-	-	65.83	-	1.32	10.43	4.28	-	-	16.72	98.58
13	S7.11.8	-	-	66.40	-	-	7.24	5.46	1.53	0.31	16.07	97.01
14	S7.8.21	-	-	65.12	-	-	9.31	4.3	0.78	1.69	16.48	97.68
15	S7.1.3	1.12	-	66.95	-	-	5.22	7.45	0.45	-	17.14	98.33
	Guettardite-twinnite, $Pb(As,Sb)_2S_4$											
16	S7.6.7	-	-	45.62	-	-	13.27	16.84	-	0.32	22.27	98.32
17	S7.a5.5	-	0.41	39.79	-	-	15.07	19.41	-	0.56	23.58	98.82

Formula	% Bnn	Formula	% Jord
1. $Cu_{0.83}Pb_{0.94}(As_{0.78}Sb_{0.35}Bi_{0.01})_{1.14}(S_{3.09}Te_{0.09})_{3.09}$	30.4	9. $Pb_{14.23}Ag_{0.07}Fe_{0.10}(As_{5.92}Bi_{0.03})_{5.95}(S_{22.65}Se_{0.10})_{22.75}$	0.0
2. $Cu_{0.93}Pb_{1.07}(Sb_{0.62}As_{0.36})_{0.99}(S_{2.94}Te_{0.04})_{2.98}$	63.1	10. $Pb_{14.14}(As_{4.68}Sb_{1.42})_{6.09}(S_{22.44}Te_{0.10}Se_{0.22})_{22.44}$	23.3
3. $Cu_{0.90}Pb_{0.92}(Sb_{0.87}As_{0.21})_{1.08}(S_{2.89}Te_{0.09}Se_{0.04})_{3.03}$	80.3	11. $Pb_{14.09}(As_{3.47}Sb_{2.67})_{6.14}(S_{22.16}Te_{0.35}Se_{0.26})_{22.77}$	43.5
4. $Cu_{0.96}Pb_{0.98}(Sb_{0.90}As_{0.13})_{1.03}(S_{3.00}Te_{0.02}Se_{0.02})_{3.04}$	86.9	12. $Pb_{13.82}(Sb_{3.73}As_{2.49}Bi_{0.27})_{6.49}S_{22.69}$	57.5
5. $Cu_{0.97}Pb_{1.02}(Sb_{0.72}As_{0.32})_{1.04}(S_{2.87}Te_{0.03}Se_{0.06})_{2.96}$	69.1	13. $Pb_{14.21}(As_{3.23}Sb_{2.64})_{5.87}(S_{22.22}Te_{0.53}Se_{0.17})_{22.92}$	44.9
6. $Cu_{0.94}Pb_{0.94}(Sb_{0.85}As_{0.16}Bi_{0.03})_{1.04}(S_{2.92}Te_{0.08}Se_{0.07})_{3.06}$	81.8	14. $Pb_{13.66}(Sb_{3.32}As_{2.49})_{5.82}(S_{22.33}Te_{0.27}Se_{0.93})_{23.53}$	57.1
7. $Cu_{1.10}Pb_{1.00}(As_{0.70}Sb_{0.32})_{1.02}(S_{2.82}Te_{0.01}Se_{0.05})_{2.87}$	31.3	15. $Pb_{13.70}Ag_{0.44}(As_{4.22}Sb_{1.82})_{6.04}(S_{22.67}Te_{0.15})_{22.82}$	30.1
8. $Cu_{1.02}Pb_{1.04}(As_{0.82}Sb_{0.24})_{1.06}(S_{2.81}Se_{0.08})_{2.88}$	22.4		
	% $PbSb_2S_4$		% $PbSb_2S_4$
16. $Pb_{1.23}(As_{1.26}Sb_{0.61})_{1.87}(S_{3.88}Se_{0.02})_{3.90}$	32.7	17. $Pb_{1.02}Cu_{0.03}(As_{1.37}Sb_{0.65})_{2.02}(S_{3.89}Se_{0.04})_{3.93}$	32.3

Sb- and As-sulphosalt mineralogy

The species of Sb- and As-sulphosalts in our sample suite (Table 3; Fig. 2) are very similar to those documented from veins elsewhere in the deposit (Ciobanu et al., 2004).

Tetrahedrite-tennantite is, however, more abundant in the salad specimens. We observe compositions across the full range of the series, with the exception of end-member tennantite. Minor amounts of *goldfieldite* are noted as inclusions in pyrite, including an unusual Pb-Bi-rich variety.

Compositions in both the *bournonite-seligmannite* and *jordanite-geocronite* series span the majority of compositions within each series, but with As-rich compositions generally sparse or absent in most samples.

In addition, we also note the occurrence of sulphosalt species in the $PbSb_2S_4$-$PbAs_2S_4$ (guettardite-sartorite) and $Pb_2Sb_2S_5$-$Pb_2As_2S_5$ (dufrenoysite) series, again similar to that in the vein assemblages (Ciobanu et al., 2004).

Bi-sulphosalt mineralogy

The Bi-sulphosalts occur only as small inclusions in pyrite and tetrahedrite (Fig. 3A, B), thus contrasting with the other types of sulphosalts that are major mineral components of the salband. Most Bi-sulphosalts are small and may be intergrown with one another or with galena. These facts are reflected in our set of microanalytical data (Table 4; Fig. 4) which display broad clusters and make it difficult to pinpoint the identity of some species.

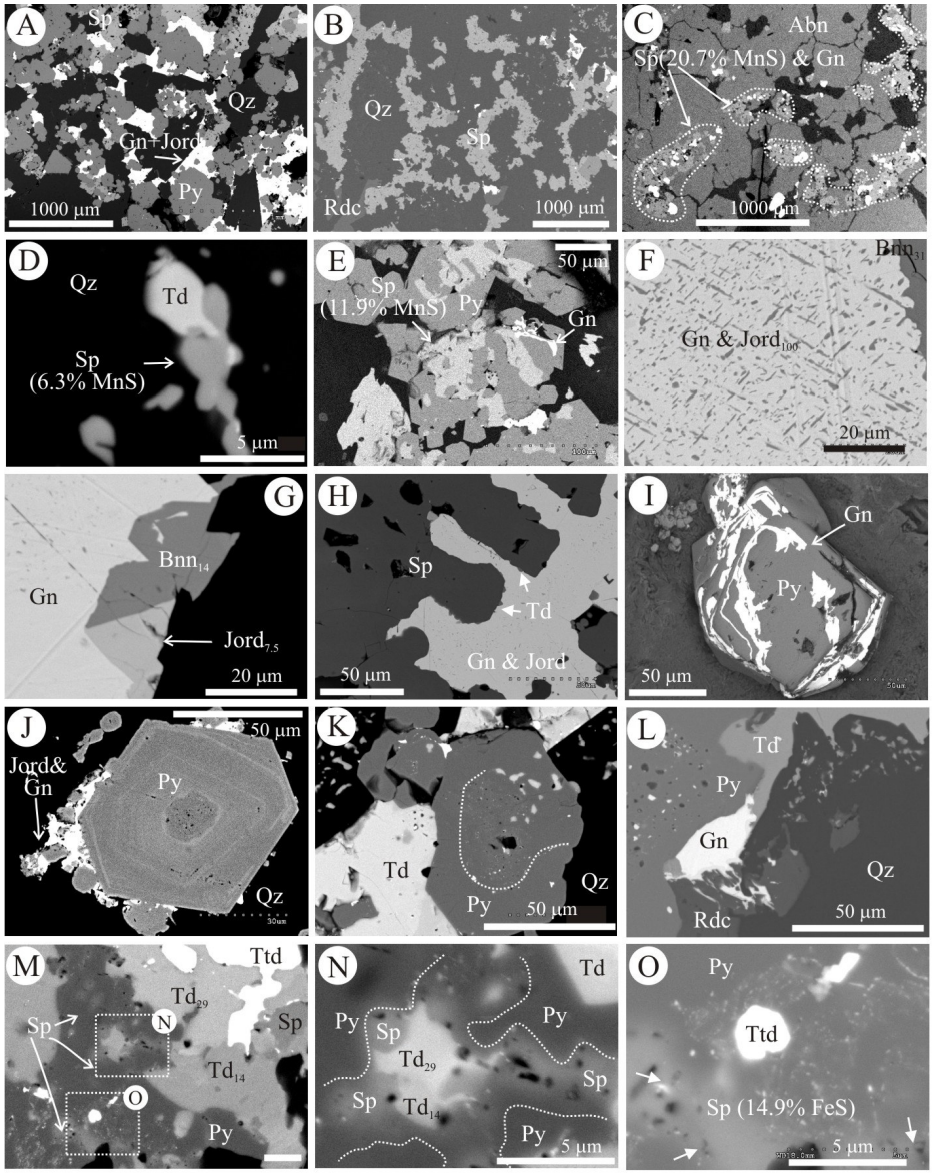

Fig. 1. Back-scattered electron images illustrating textural relationships in salband ore. A (7.1), B (7.8), C (7.3): Mottled textures between different sulphides and/or gangue minerals; D) Bleb composed of Sp and Td in Qz (7.3). E) Py replaced by Sp, note the spiral shape of Sp in the upper grain indicative of rotation (7.6). F) Exsolutions of Jord in Gn (7.2). G) Twinned sulphosalts at the margin of Gn with scarce Jord exsolutions (7.7). H) Replacement of Sp by Gn following initial carries texture (7.2). I) Gn replacing growth zones in Py (7.6). J). Growth pattern in Py marked by As-bearing zones (light). (7.8). K) (7.2), L) (7.5) Emulsion-like textures realised by blebs of Td in Py (K) and Qz (L). Note the sinusoidal boundary between Td and Py indicative of shear assisted deformation (L). M, N, and O) Diffusion of Sp within Py. Note the fluid inclusion trails (arrowed) and presence of tellurides in the same areas (7.5). Abbreviations are given in Table 1

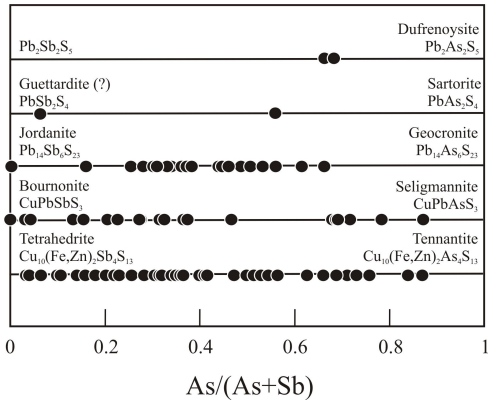

Fig. 2. Compositional variation among Sb- and As-sulphosalts

Cosalite ($Pb_2Bi_2S_5$), *aikinite* ($CuPbBiS_3$), and *galenobismutite* ($PbBi_2S_4$) are noted in minor amounts. In addition, we also mention the occurrence of what we believe is *nuffieldite*, an unidentified Ag-Cu-Pb-Bi sulphosalt, with composition close to *$AgCuPbBi_2S_5$*, and also a phase highly reminiscent of a *Cu-Pb-rich pavonite homologue* (Table 3). Cosalite grains tend to be idiomorphic and may include thin lamellae of Pb_3BiTeS_4 (Fig. 3C). Some of these rare sulphosalts are found within the fields of inclusions in pyrite mostly dominated by fahlore, chalcocite or a combination of both (Fig. 3A). In rare cases, these phases are associated with Bi-sulphosalts, like the nuffieldite (?) in Fig. 3D. Galena, one of the common components in the inclusions (Fig. 3B) can also be present as fine strips within larger grains of aikinite (Fig. 3E). Sub-micron intergrowths of galena within aikinite may explain the offset of the compositional cluster corresponding to this mineral (Fig. 4).

The most abundant species are, however, *lillianite homologues* (Fig. 3F-H). Our data cluster between the N = 4 (lillianite-gustavite) and N = 7 (heyrovskyite) compositional tie lines, but also extend towards Ag- and Pb-rich compositions suggestive of fine-grained intergrowths with galena-matildite. Modest Sb and Se contents are noted in some grains. Bleb-shapes, as in Fig. 3F, indicate deposition in dilational sites within pyrite. Typical lamellar texture with slight compositional differences (Fig. 3G) is most indicative of microscopic intergrowths between lillianite homologues and/or members of galena-matildite series (see below). Pb_3BiTeS_4 and buckhornite are found as inclusions as well within this same grain. The presence of emulsion-like blebs composed of galena and Ag-rich lillianite homologues indicates precipitation above solvus of this assemblage (Fig. 3H).

The *matildite* ($AgBiS_2$) - *galena* (PbS) series is represented by relatively abundant inclusions (Fig. 3I-K). Some show decomposition to galena, matildite and one or the intermediate phases (Fig. 3I) obtained synthetically in the system Pb-Ag-S at temperatures as low as 144ºC (Wang, 1999). Interestingly, homogeneous grains with compositions approximating to three of the five intermediate synthetic phases in the series ($PbAg_2Bi_2S_5$ (Fig. 3I, J), $Pb_4Ag_{5.6}Bi_{5.6}S_{15.2}$ and $PbAgBiS_3$) are noted. Intermediate members of this series are reported from a number of vein occurrences, e.g., Karamazar, Russia (Bortnikov et al., 1987); Colorado, California and Pennsylvania, USA (Foord and Shawe, 1989), Stiavnika-Hodrusa, Slovakia (Kovalenker et al., 1993).

Discussion

Based upon textural relationships (Fig. 1), we interpret that pyrite, alabandite and fahlores are deposited first, followed by sphalerite and Bnn-Sel, and lastly by galena and Jord-Gcn. Even though such a deposition sequence indicates a metal compositional shift from Fe-(Mn)-Cu- to Zn-Cu-Pb- to Pb-rich, a complex polymetallic character of the ore precipitates is, however, strongly suggested for all stages. This is seen not only by the ubiquitous presence of Sb-(As)-sulphosalts, but also in the range of mottled and exsolution textures spanning the entire sequence. Compositional trends, as exemplified by the pair sphalerite-alabandite, are evidence that mottled textures are genetically indicative of co-precipitation of the minerals involved. Sequential co-precipitation of the sulphide/ sulphosalt associations in the salband parallels

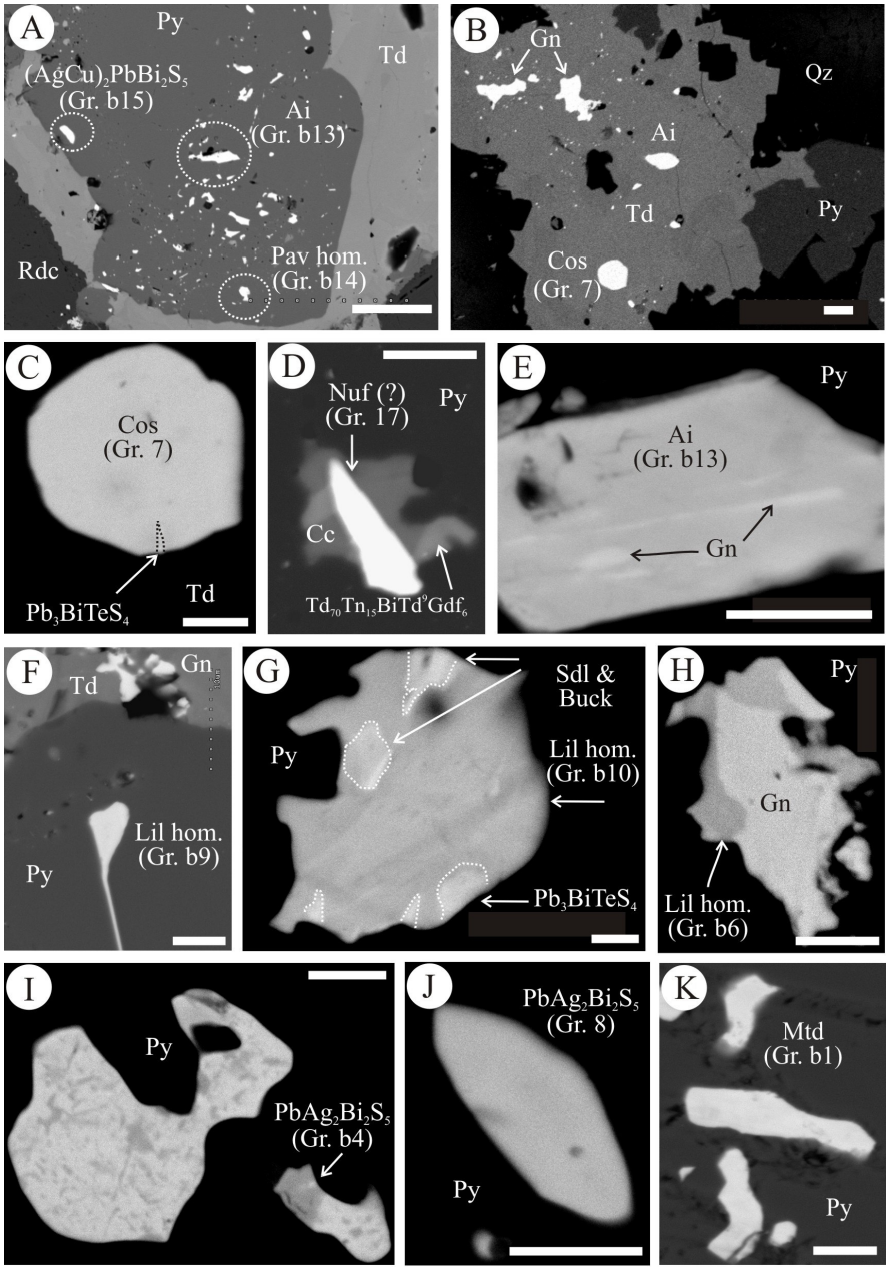

Fig. 3. Back-scattered electron images illustrating the occurrence of Bi-sulphosalts in salband ores from Sacarimb. See text and table for additional description and explanation. All scale bars 5 µm, except (A): 50 µm. Abbreviations: Ai: aikinite, Alek: aleksite group phase, Buck: buckhornite, Cc: chalcocite, Cos: cosalite, Gn: galena, Lil hom.: lillianite homologue, Mtd: matildite, Nuf: nuffieldite, Pav hom.: pavonite homologue, Py: pyrite, Qz: quartz, Rdc: rhodochrosite, Td: tetrahedrite

Table 4. Representative compositions of Bi-sulphosalts, Sacarimb. Brackets indicate mean (n)

	Ag	Cu	Pb	Bi	Sb	Te	Se	S	Total	Formula
(Ag)-Pb-Bi-sulphosalts										
Galenobismutite										
S7.5 gr.11 (2)	0.35	1.40	21.20	58.53	0.27	0.55	0.83	18.24	101.23	$(Pb_{0.72}Cu_{0.16}Ag_{0.02}Bi_{1.97}Sb_{0.02})_{2.89}(S_{4.01}Se_{0.07}Te_{0.03})_{4.11}$
Cosalite										
S7.5 gr.7	0.88	-	40.64	39.87	1.75	-	1.18	14.85	99.16	$(Pb_{1.99}Ag_{0.08}Bi_{1.93}Sb_{0.15})_{4.15}(S_{4.70}Se_{0.15})_{4.85}$
S7.5 gr.6	1.13	-	43.05	27.03	6.93	-	-	17.74	95.90	$(Pb_{1.95}Ag_{0.10}Bi_{1.21}Sb_{0.53})_{3.80}S_{5.20}$
Lillianite homologues										
S7.5 gr.b6 (6)	5.15	2.12	42.18	29.10	4.70	0.34	1.07	14.96	99.62	$Ag_{0.55}Cu_{0.39}Pb_{2.37}Bi_{1.62}Sb_{0.45}(S_{4.43}Se_{0.16}Te_{0.03})_{5.62}$
S7.5 gr.b7 (5)	1.24	3.91	47.62	27.83	0.70	1.05	0.75	14.76	97.85	$Ag_{0.14}Cu_{0.74}Pb_{2.75}Bi_{1.59}Sb_{0.09}(S_{5.51}Se_{0.11}Te_{0.10})_{5.72}$
S7.5 gr.b10 (5)	6.11	-	45.43	29.81	1.04	0.28	1.29	14.23	98.19	$Ag_{0.70}Pb_{2.71}Bi_{1.76}Sb_{0.11}(S_{5.49}Se_{0.20}Te_{0.03})_{5.72}$
S7.5 gr.b12 (2)	4.43	0.76	48.36	29.98	1.44	0.82	0.67	13.80	98.26	$Ag_{0.51}Cu_{0.15}Pb_{2.93}Bi_{1.68}Sb_{0.15}(S_{5.40}Se_{0.11}Te_{0.08})_{5.58}$
Matildite-galena series (close to end-member $AgBiS_2$)										
S7.5 gr.b1 (4)	25.91	0.86	6.45	48.16	-	0.47	4.81	13.47	100.13	$Ag_{0.96}Cu_{0.05}Pb_{0.12}Bi_{0.92}(S_{1.68}Se_{0.24}Te_{0.01})_{1.94}$
Matildite-galena series (close to $PbAg_2Bi_2S_5$)										
S7.5 gr. 8 (4)	21.38	1.54	13.19	47.47	0.48	0.49	0.35	15.63	100.55	$Ag_{1.96}Cu_{0.24}Pb_{0.63}Bi_{2.24}Sb_{0.04}(S_{4.81}Se_{0.04}Te_{0.04})_{4.89}$
Matildite-galena series (close to $Pb_4Ag_{5.6}Bi_{5.6}S_{15.2}$)										
S7.5 gr. 9	21.41	-	26.45	33.21	-	-	0.85	15.16	97.09	$Ag_{6.23}Pb_{4.01}Bi_{4.99}(S_{14.84}Se_{0.34})_{15.18}$
Matildite-galena series (close to $PbAgBiS_3$)										
S7.5 gr.b3	19.14	0.91	32.76	28.22	-	0.63	0.60	14.20	96.47	$Ag_{1.12}Cu_{0.09}Pb_{1.01}Bi_{0.86}(S_{2.83}Se_{0.05}Te_{0.03})_{2.91}$
Cu-Pb-Bi- and Cu-Ag-Pb-Bi-sulphosalts										
Aikinite										
S7.9 gr.11 (2)	0.89	10.13	33.86	35.43	-	-	0.49	15.58	96.40	$Pb_{0.99}Ag_{0.05}Cu_{0.96}Bi_{1.02}(S_{2.94}Se_{0.04})_{2.98}$
Nuffieldite (?)										
S7.5 gr.17	3.16	6.82	31.89	33.52	3.58	-	0.94	16.53	96.43	$Ag_{0.38}Cu_{1.38}Pb_{1.99}Bi_{2.07}Sb_{0.38}(S_{6.65}Se_{0.15})_{6.80}$
Cu-Pb rich pavonite homologue (?)										
S7.5 gr.20	4.94	4.48	14.49	59.64	-	-	-	16.13	99.68	$Ag_{0.47}Cu_{0.72}Pb_{0.72}Bi_{2.93}S_{5.16}$
S7.5 gr.b14 (4)	5.79	5.10	13.47	58.34	0.41	0.17	4.97	14.22	102.87	$Ag_{0.54}Cu_{0.87}Pb_{0.65}Bi_{2.80}Sb_{0.03}(S_{4.46}Se_{0.63}Te_{0.01})_{5.10}$
Ag-Cu-Pb-Bi sulphosalt ~$AgCuPbBi_2S_5$										
S7.5 gr.18 (5)	10.75	6.91	18.86	47.17	0.17	0.17	0.19	15.53	99.98	$Ag_{0.98}Cu_{1.07}Pb_{0.89}Bi_{2.22}Sb_{0.01}(S_{4.76}Se_{0.05}Te_{0.01})_{4.83}$
S7.5 gr.15 (3)	7.83	5.40	24.17	44.57	0.10	0.13	5.96	13.28	101.44	$Ag_{0.74}Cu_{0.87}Pb_{1.19}Bi_{2.18}Sb_{0.01}(S_{4.23}Se_{0.77}Te_{0.01})_{5.01}$

trends in telluride/sulphosalt associations from the vein filling (Ciobanu et al., 2004). Release of each batch of precipitate from the fluids is accompanied by partial replacement of previously-formed grains. Like in the main ore, shear-assisted brecciation and syn-deformational deposition is characteristic of the veins at Sacarimb. The extent of emulsion-like halos surrounding sulphide/sulphosalts formed during episodes of brecciation is indicative of vein reopening. Such halos represent selvages between new-formed quartz and/or rhodochrosite and ore minerals. Similar textures, with native Au present in such halos, were also observed in the main ore, even though limited to samples where rhodochrosite is abundant. Reopening of the veins and intense brecciation is accompanied by precipitation of Bi-sulphosalts and also telluride deposition.

This is the second occurrence of Bi-sulphosalts in the Golden Quadrilateral confirmed by microanalysis. The first is known from deeper levels of Larga-Fata Baii veins (Cook and Ciobanu, 2004), thus contrasting with Sacarimb where it appears at the upper levels of the veins.

Experimental work in the Ag_2S-PbS-Bi_2S_3 system shows that the intermediate range in the PbS-$AgBiS_2$ solid solution series persists down to 200ºC, and formation of discrete members within this range were obtained at temperatures down to 144ºC (Wang, 1999). The gustavite-lillianite solid solution series, however, is confirmed by the same study in the interval 350-450ºC. Hence, we consider the latter as constraining the upper limit for deposition of Bi-sulphosalts, since Ag-rich lillianite homologues are the most abundant type of Bi-sulphosalt found in this study. Temperatures of only ~ 300ºC were estimated for the main stage

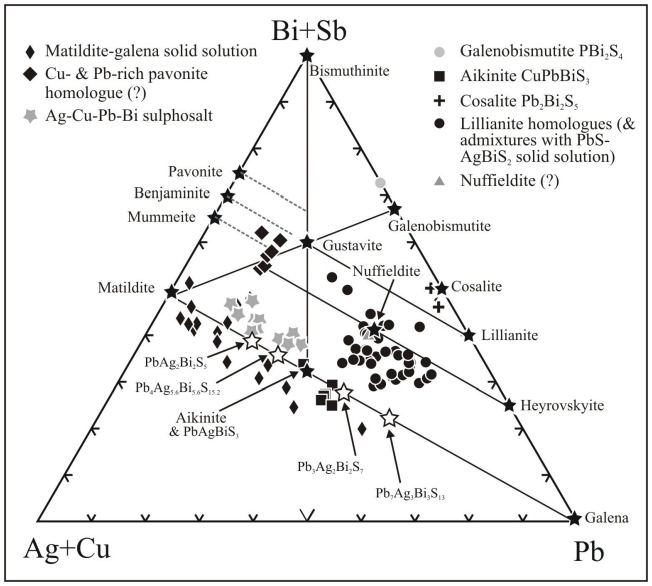

Fig. 4. Compositional variation in Bi-sulphosalts, projected onto the (Ag+Cu)-Pb-Bi ternary diagram

of telluride mineralization based on fluid inclusions studies (Alderton and Fallick, 2000), and phase relationships in the Au-Ag-Te system (Ciobanu et al., 2004). Thus, on the basis of Bi-sulphosalts speciation in the salband, we suggest that reopening of some parts of the veins introduced fluids of temperatures of at least 50ºC higher than those producing the main telluride stage at Sacarimb.

Conclusions

1. Sb- and As-sulphosalts are major phases in the salband mineralization at Sacarimb.
2. We confirm the presence of several types of Bi-sulphosalts in the Sacarimb deposit. The minerals are minor constituents of the ore.
3. The unusually diverse chemistry of the Sacarimb deposit is also reflected in the compositions of the sulphosalts.
4. Sulphosalts are, in effect, the main Au-carriers in the salband as they are the main host for fine-grained Au-(Ag) tellurides.

References

Alderton, D.H.M., Fallick, A.E. 2000. The nature and genesis of gold-silver-tellurium mineralization in the Metaliferi Mountains of western Romania. *Economic Geology*, **95**, 495-515.

Bortnikov, N.S., Laputina, I.P., Safonov, Yu.G. 1987. New mineral group of the system Ag-Pb-Bi-S from Kanimansur ore field, Karamazar. *Dokl. Akad. Sci. USSR, Earth Sci. Sect.* **292**, 1459-1463.

Ciobanu, C.L., Cook, N.J., Damian, G., Damian, F., Buia, G. 2004. Telluride and sulphosalt associations at Sacarimb. In: N.J. Cook, C.L. Ciobanu (Eds.), *Au-Ag Telluride Deposits of the Golden Quadrilateral, South Apuseni Mts., Romania.* IAGOD Guidebook Series, **12**, 145-186.

Cook, N.J., Ciobanu, C.L. 2004. Bismuth tellurides and sulphosalts from the Larga hydrothermal system, Metaliferi Mts., Romania: Paragenesis and genetic significance. *Mineralogical Magazine*, **68**, 301-321.

Foord, E.E., Shawe, D.R. 1989. The Pb-Bi-Ag-Cu-(Hg) chemistry of galena and some associated sulphosalts: A review and some new data from Colorado, California and Pennsylvania. *Canadian Mineralogist,* **27***,* 363-382.

Kovalenker, V., Jelen, S., Sandomirskaya, S. 1993. Minerals of the system Ag-Cu-Pb-Bi-S from the polymetallic veins of the Stiavnica-Hodrusa ore field (Slovakia). *Geol. Carpathica*, **44**, 409-419.

Wang, N. 1999. An experimental study of some solid solutions in the system Ag_2S-PbS-Bi_2S_3 at low temperatures. *N. Jahrb. Mineral. Monatsh.*, 223-240.